
Plan, Verify and Fill: A Structured Parallel Decoding Approach for Diffusion Language Models

Miao Li^{*1} Hanyang Jiang^{*1} Sikai Cheng¹ Hengyu Fu² Yuhang Cai² Baihe Huang² Tinghan Ye¹
 Xuanzhou Chen¹ Pascal Van Hentenryck¹

Abstract

Diffusion Language Models (DLMs) present a promising non-sequential paradigm for text generation, distinct from standard autoregressive (AR) approaches. However, current decoding schemes often adopt a conservative strategy by decoding only high-confidence tokens, underutilizing the global bidirectional context to guide global trajectories. Motivated by the empirical observation that structurally salient tokens tend to be more reliable than arbitrary tokens, we propose Plan-Verify-Fill (PVF), a training-free paradigm that grounds planning via quantitative validation. PVF actively constructs a hierarchical skeleton by prioritizing high-leverage semantic anchors and employs a verification protocol to operationalize pragmatic structural stopping, where further deliberation yields diminishing returns. Extensive evaluations on LLaDA-8B-Instruct and Dream-7B-Instruct demonstrate that PVF reduces the Number of Function Evaluations (NFE) by up to 65% compared to confidence-based parallel decoding across benchmark datasets, unlocking superior efficiency without compromising accuracy.

1. Introduction

DLMs (Gong et al., 2024; Shi et al., 2024; Lou et al., 2024; Ye et al., 2025a; Nie et al., 2025) extend the iterative denoising paradigm of diffusion models to discrete text generation, offering an alternative to the strictly sequential decoding employed by AR models. By operating over a global canvas and iteratively refining token predictions, DLMs unlock substantial potential for parallel token updates. This global representation further enables reasoning over long-range

structure and planning dependencies across the sequence (Li et al., 2022). Recent studies, together with real-world deployments (Khanna et al., 2025; Nie et al., 2025; Ye et al., 2025a; Google DeepMind, 2025), demonstrate that masked diffusion architectures scale well and deliver competitive performance across a range of tasks.

This same flexibility also introduces new challenges. By relaxing the strict left-to-right decoding constraint, DLMs expand the space of admissible decoding orders, with AR generation as a special case within this broader framework. From this perspective, DLMs can be interpreted as any-order AR models (Ou et al., 2024; Hoogeboom et al., 2021). While this enlarged space may enable generation orders that better align with task structure, it also admits many trajectories that poorly match the natural sequential organization of language (the *curse of parallel decoding* (Wu et al., 2025b)), highlighting a fundamental challenge:

How can we identify decoding trajectories that are both reliable and capable of fully unleashing the theoretical potential of parallel decoding?

In practice, many existing decoding strategies address this challenge conservatively with confidence-based strategies (Gong et al., 2024; Chang et al., 2022; Ye et al., 2025a; Wu et al., 2025b). These strategies focus on securing “safest bets”: locking in tokens as soon as they reach certain confidence threshold. While this heuristic is effective for parallel decoding, it reacts passively towards global structure, waiting for complex dependencies to emerge. Consequently, the decoding process risks settling into the path of least resistance, failing to fully leverage the diffusion framework’s unique capacity to actively coordinate long-range decisions.

To overcome this limitation, a promising avenue is to design decoding strategies that explicitly leverage the intrinsic structural foresight of underlying language models (LMs). Emerging evidence suggests that semantic construction in LMs is not a uniform flow, but rather a rhythmic process punctuated by sparse, high-leverage decision points that shape global generation trajectories (Wang et al., 2025a; Cheng et al., 2025; Zhang et al., 2023; Bogdan et al., 2025; Ye et al., 2025b; Wang et al., 2023). Mechanistic interpretations substantiate this view: Li et al. (2025b) demonstrates

¹Department of H. Milton Stewart School of Industrial and Systems Engineering, Georgia Institute of Technology, Atlanta, USA ²University of California, Berkeley, USA. Correspondence to: Miao Li <mli746@gatech.edu>, Hanyang Jiang <scot-tjhy@gatech.edu>.

that attention dynamics encode a “mechanistic blueprint” of reasoning roles, rendering the model’s internal logic legible not merely as a byproduct of computation.

Motivated by these insights, an appealing direction is to explore *structural control tokens* as high-impact anchors for guiding DLM decoding trajectories. Empirically, we find that a curated vocabulary of content-neutral structural markers (e.g., “Therefore” and “Firstly”) is consistently safer to commit at lower confidence than arbitrary tokens, suggesting a decoding strategy that exploits this asymmetry.

Therefore, we propose **Plan-Verify-Fill (PVF)** to operationalize active structural steering within the decoding process. PVF employs a dual-route architecture to decouple high-level skeleton generation from fine-grained filling. The **Planning Route** proactively injects “planning tokens” to guide the global trajectory, while a rigorous **Verification Mechanism**, based on the *impact set*, ensures these “bold” structural commitments remain mathematically consistent with the model’s latent consensus. When structural planning yields diminishing returns, an **AR Fallback Route** executes dense content resolution. This mechanism rapidly fills blank spans to densify and stabilize the local conditioning context, causing the latent structural scaffold targeted by planning to emerge earlier. Together, these components enable planning-aware decoding without sacrificing robustness.

Empirically, our analysis suggests that actively regulating the planning horizon leads to superior decoding efficiency. We evaluate PVF on six benchmarks with LLaDA-8B-Instruct and Dream-7B-Instruct, to demonstrate model-agnostic robustness. By proactively securing high-leverage anchors, PVF breaks the bottleneck of confidence-based strategies, achieving NFE reductions of over 60% on GSM8K, MMLU-Pro, ARC-C and WinoGrande, and over 40% on complex reasoning tasks compared to strong baselines like Fast-dLLM (Wu et al., 2025b;a) and Free-Dave (Wu & Zhang, 2025). Our contributions can be summarized as follows:

- We introduce **PVF**, a training-free, model-agnostic parallel decoding strategy that shifts generation from reactive token harvesting to active planning, locking in a hierarchical skeleton via discourse scaffolds before refining local content.
- A Consistency Verification protocol, formalized via impact sets, that enforces validity constraints on all steering decisions, ensuring structural commitments remain mathematically consistent with the model’s latent consensus *without degrading final decoding accuracy*.
- To the best of our knowledge, PVF is among the first approaches to incorporate semantic cues as an explicit decision signal in DLM parallel decoding, surpassing reliance on token probabilities alone.

1.1. Related Work

Parallel Decoding The scalability of global denoising has enabled the rise of DLMs (Nie et al., 2025; Ye et al., 2025a; Zhu et al., 2025), which rival AR baselines in performance while offering massively parallel inference (Prabhudesai et al., 2025). To harness this potential, recent studies have explored hybrid block-wise diffusion (Chen et al., 2024; Ariola et al., 2025; Nie et al., 2025), merging autoregressive flexibility with parallel throughput. Algorithmically, strategies have evolved from rigid schedules (Chang et al., 2022) to adaptive strategies (Yu et al., 2025; Wu et al., 2025b; Fu et al., 2025; Ben-Hamu et al., 2025; Wu & Zhang, 2025) that leverage position-specific calibration and uncertainty-driven exploration for more efficient decoding.

Token-Level Planning Signals Recent investigations reveal that the locus of planning is intrinsically tied to discrete semantic units. Zhang et al. (2023) utilizes math operation tokens to abstract macro-level logic. Similarly, Wang et al. (2025a); Cheng et al. (2025); Bogdan et al. (2025) identify high-leverage components as “Thought Anchors”—sparse linguistic triggers that actively steer the global reasoning trajectory. Expanding on this hierarchical view, both Wang et al. (2023) and Zhou et al. (2025) demonstrate that self-defined special tokens can be trained to encapsulate the semantic essence of planning, serving as a self-defined map for the generation process. Inspired by this distinction, we operationalize these repetitive structural scaffolds as stable cognitive anchors in PVF, offering a low-uncertainty foundation upon which more volatile semantic reasoning can be safely constructed.

Hierarchy-aware decoding for DLMs In this work, we classify strategies that separate structural planning from content realization as hierarchical-structure-aware decoding. This paradigm has evolved from early latent refinement methods (Li et al., 2022) to explicit separations, such as the semantic scales (Zhou et al., 2025) and the planner-executor framework of Berrayana et al. (2025). Closest to our approach are Israel et al. (2025), which uses an AR phase to lock in structural control tags, and Li et al. (2025a), which identifies structural chunks using data-driven thresholds. PVF distinguishes itself by synergizing semantic intent with statistical rigor. Unlike the upfront commitments of Israel et al. (2025), PVF adopts an iterative approach that evolves the structural plan as the context matures, effectively reducing the reliance on precise upfront planning. Furthermore, in contrast to the purely statistical proxies of Li et al. (2025a), PVF employs a dual certification protocol: anchors must be both semantically significant and statistically stable. This allows PVF to detect the point of structural saturation, while remaining a lightweight solution that avoids the retraining overhead of prior studies.

2. Preliminary

Departing from the left-to-right decoding of AR models, DLMS (Austin et al., 2021; Lou et al., 2023; Ou et al., 2024) recast generation as an iterative refinement task. This framework adapts diffusion principles to the discrete domain via two governing dynamics: a forward process that systematically corrupts the sequence by masking tokens, and a parameterized reverse process trained to recover the original text from the corrupted state.

Forward Process (Corruption): The forward process $q(\mathbf{x}_s|\mathbf{x}_0)$ defines a transition distribution that progressively corrupts the clean data vector \mathbf{x}_0 over time $s \in [0, 1]$. In this framework, tokens are replaced by a special mask token [MASK], which serves as an *absorbing state*—once a token becomes masked, it remains masked throughout the process. Consequently, the clean sequence \mathbf{x}_0 is gradually transformed into a fully masked sequence at \mathbf{x}_1 . In other words, this process is defined by the transition probability, following the notation in (Austin et al., 2021):

$$q(\mathbf{x}_s|\mathbf{x}_0) = \prod_{i=1}^{|\mathbf{x}_0|} q(x_s^i|x_0^i) = \prod_{i=1}^{|\mathbf{x}_0|} \text{Cat}\left(x_s^i; (1-s)\delta_{x_0^i} + s\delta_{[\text{MASK}]}\right).$$

Reverse Process (Denoising): Given an input sequence $\mathbf{y} = [\mathbf{y}_{\text{prompt}}, \mathbf{y}_{\text{gen}}]$, where $\mathbf{y}_{\text{prompt}}$ denotes the fixed context and $\mathbf{y}_{\text{gen}} \in \mathcal{V}^L$ represents the masked sequence to be generated over a vocabulary \mathcal{V} . The generation model P_θ is commonly trained under an ELBO-based objective (Nie et al., 2025; Sahoo et al., 2024; Ou et al., 2024), to recover clean data from corrupted states. During inference, generation proceeds by iteratively reversing the forward corruption process using the learned transition $P_\theta(\cdot | \mathbf{y}_t)$. At each timestep t , the fitted model P_θ produces a more refined estimate of the underlying clean sequence $\mathbf{y}_t = [y_t^1, \dots, y_t^L] \in \mathcal{V}^L$, where each token representation y_t^i corresponds to a categorical distribution over the vocabulary \mathcal{V} .

Confidence-based Parallel Decoding: One of the most prominent decoding strategies in DLMS is confidence-based decoding (Yu et al., 2025), which governs the generation process based on prediction certainty.

For each masked position i at step t , define the model’s top prediction \hat{y}_t^i conditioned on the previous state \mathbf{y}_{t-1} :

$$\hat{y}_t^i = \arg \max_{w \in \mathcal{V}} P_\theta(y^i = w | \mathbf{y}_{t-1}).$$

In its most canonical form, the algorithm progressively fills the sequence by committing to tokens where the model’s confidence exceeds a static threshold τ_{high} :

$$y_t^i = \begin{cases} \hat{y}_t^i, & \text{if } P_\theta(y^i = \hat{y}_t^i | \mathbf{y}_{t-1}) \geq \tau_{\text{high}}, \\ y_{t-1}^i, & \text{otherwise.} \end{cases} \quad (1)$$

While this static heuristic serves as a basic building block for parallel decoding, later approaches (Wu et al., 2025b; Fu et al., 2025; Chen et al., 2025; Jin et al., 2025; Lou et al., 2024) adopt more complex decoding mechanisms that extend beyond heuristic gating, enabling adaptive control over diffusion steps for efficient parallel generation.

Semi-Autoregressive Blockwise Decoding Semi-AR diffusion adopts a hybrid structure combining *inter-block* autoregression with *intra-block* parallel diffusion. Widely adopted in modern DLMS (Arriola et al., 2025; Ye et al., 2025a; Nie et al., 2025; Sahoo et al., 2024; Wu et al., 2025a;b), this strategy restricts attention to local regions, thereby reducing inference cost while preserving the local context. First partition the fixed canvas length L into B blocks, writing $\mathbf{y}_t = [y_t^{1:L/b}, y_t^{L/b+1:2(L/b)}, \dots, y_t^{L-b+1:L}]$. The k -th block encompasses the token segment spanning from index $(k-1)\frac{L}{B} + 1$ to $k\frac{L}{B}$. During inference, the decoding process adheres to a block-causal constraint: the state \mathbf{y}_t can commit tokens in the $(k+1)$ -th block only if the k -th block is fully resolved (i.e., contains no [MASK] tokens); otherwise, all subsequent blocks $j > k$ must remain strictly masked. In this paper, we follow the framework of semi-autoregressive blockwise decoding. We define \mathcal{B}_t to represent the set of indices for the current *working block(s)* where [MASK] tokens are eligible for replacement at step t .

3. Inducing Hierarchical Structure with Planning Tokens

Prior work shows that adaptively lowering the confidence threshold can substantially accelerate diffusion decoding with limited accuracy loss (Wu et al., 2025b). This raises a natural question:

Are all lower-confidence tokens, based primarily on a probabilistic threshold, equally safe to commit, or are some intrinsically safer to decode early? For example, when multiple candidates fall within the same low-confidence band near the threshold, does the specific choice among them matter?

This question is especially salient for DLMS because decoding requires navigating an enormous search space: unlike AR models that collapse uncertainty sequentially, DLMS must jointly resolve both *what* to say (content generation) and *how* to organize it (structural planning) across a global canvas. To answer this question, we examine token-level confidence dynamics and find empirically that low-confidence tokens vary substantially in reliability: *planning tokens*, a small set of structurally salient anchors, can often be committed early at lower confidence with noticeably smaller degradation in accuracy.

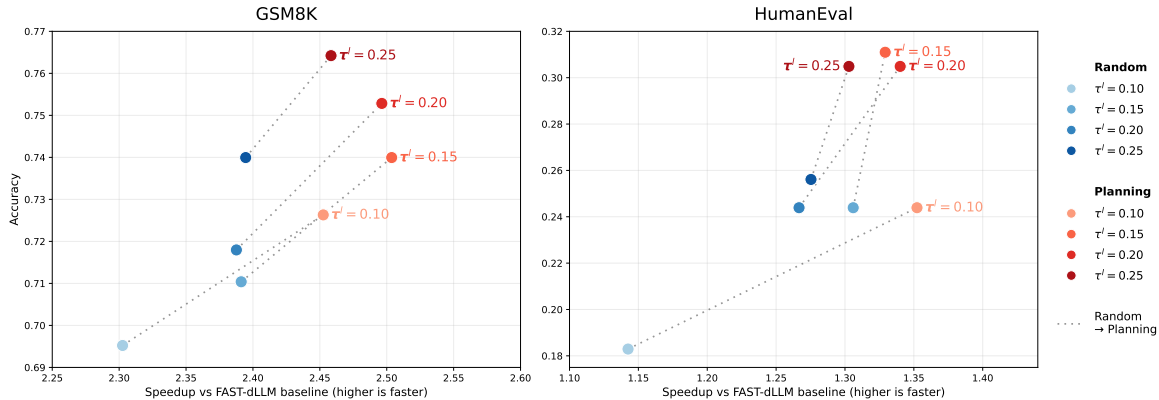


Figure 1. Ablation on GSM8K and HumanEval comparing lower-confidence commits of planning tokens versus random tokens (i.e., without prioritizing planning tokens). Across confidence bins, prioritizing planning tokens consistently yields faster decoding and improved accuracy; points closer to the upper-right indicate better performance on both axes.

The Safety of Content-Neutral Anchors. A natural concern with forcing low-confidence tokens is the risk of “hallucination” or error propagation. Here, we distinguish between *Content Risk* and *Structural Risk*.

- **Content Forcing (High Risk):** Forcing a dense content token (e.g., a specific number like “7” or a variable name) when confidence is low is dangerous. If the model is unsure, forcing a specific value creates a factual premise that may lead to an error.
- **Structure Forcing (Low Risk):** In contrast, Planning Tokens are largely *content-neutral*. Forcing a logical connector like “Therefore” does not assert a fact; instead, it mainly imposes a *topological constraint*.

Restricting Search Space via Structural Constraints. Content generation is inherently instance-specific, so many fine-grained details are difficult to settle early. Structural cues, in contrast, are more consistent across instances (e.g., `def` and `return` in code, `recur` broadly), motivating us to examine whether they can be committed earlier. This asymmetry is important because low confidence does not necessarily reflect missing knowledge: it could arise from *trajectory ambiguity*, where probability mass is split across competing trajectories and certainty consolidates slowly.

We leverage this asymmetry to explore a simple intervention: prioritizing the commitment of *Planning Tokens*, a specialized subset of the vocabulary \mathcal{P} (e.g., logical connectors such as `Therefore` and structural separators; see Sections 3.1 and A.1), to prune the search space. We hypothesize that such early structural commitments may help disambiguate competing trajectories and guide the model toward a coherent structural skeleton.

Empirically, we adopt the static variant of Fast-dLLM (Wu et al., 2025b) as the baseline. At each decoding step, in addition to the tokens selected by Fast-dLLM, we randomly commit one extra token whose confidence lies within a pre-

scribed low-confidence interval $[\tau^l, \tau^u]$. In Figure 1, we fix $\tau^u = 0.6$ for simplicity. The results show that unrestricted low-confidence commitments (labeled *Random* in Figure 1) cause substantial performance degradation, whereas prioritizing our content-neutral planning token set \mathcal{P} for such commitments (labeled *Planning* in Figure 1) markedly reduces the accuracy loss while also improving efficiency. Additional experimental details are provided in Section A.2.

3.1. Automated Discovery via Structural Distillation

Manually constructing a comprehensive planning vocabulary \mathcal{P} is intractable given the diversity of generation contexts. To address this, we utilize a modern LLM as a *structural distillation engine* to extract a compact set of *domain-invariant* tokens that serve as reusable reasoning scaffolds. Concretely, we prompt the model to identify a “structural skeleton” of valid syntax that satisfies the following criteria:

1. **High Structural Leverage:** tokens that act as frequent control anchors (e.g., logical connectives, syntactic delimiters, or control-flow keywords) and meaningfully constrain the global structure of the generation;
2. **Content Neutrality:** tokens that are agnostic to specific instances, avoiding dense content (e.g., numerical constants) while expressing relations or structure.

Additional details are provided in Section A.1.

4. Methodology: Plan-Verify-Fill (PVF) Decoding

Building upon the above findings, we propose **Plan-Verify-Fill (PVF)** (see Figure 3 for an overview), a novel decoding strategy for DLMs that leverages *planning tokens* to guide generation. In addition to parallel decoding, PVF alternates between committing high-level structural anchors via planning and applying an accelerated AR fallback to accelerate fine-grained completion. This decoupling encourages priori-

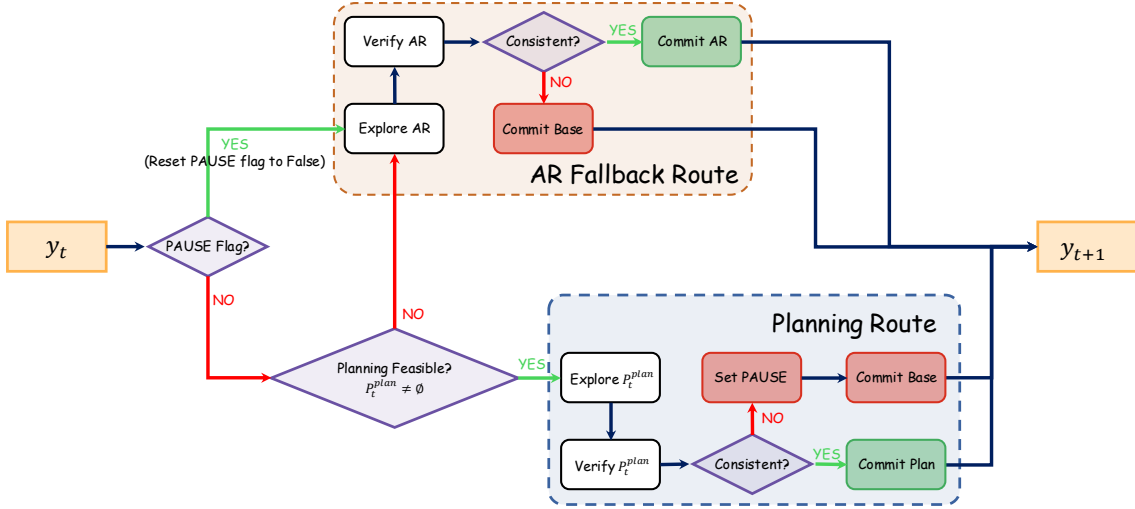


Figure 3. Overview of the **Plan-Verify-Fill (PVF)** decoding pipeline.

tizing global stabilization before fine-grained commitments, mitigating premature commits in high-uncertainty regions.

Overview of the PVF Pipeline The PVF process operates via a dual-route architecture. The primary **Planning Route** proceeds in two phases: **(1) Proposal**, where planning tokens are tentatively injected based on a lower confidence threshold τ_{plan} to encourage structural buildup; and **(2) Verification**, which enforces consistency with high-confidence parallel-decoding decisions under τ_{high} . Should this route fail, the system reverts to the **AR Fallback Route**, a secondary mechanism that bypasses planning and advances decoding via local filling with a route-specific consistency check, when planning cues are insufficient (see Figure 3). **Safeguarding Consistency through the Impact Set** While recent work shows that exploiting lower-confidence tokens is key for decoding efficiency (Fu et al., 2025; Wu & Zhang, 2025; Wu et al., 2025b; Huang et al., 2025), such commits are not uniformly safe: in some cases, a suboptimal early commitment can bias the trajectory away from valid semantic attractors. PVF addresses this risk through a verification mechanism that validates each tentative commit by checking its downstream consistency over the affected positions under a route-specific criterion.

To formalize this safety constraint, we define the *impact set* S^{impact} . Let $\mathcal{M}(\mathbf{y}) = \{i \in \mathcal{B} \mid y^i = [\text{MASK}]\}$ denote the set of indices within the target block \mathcal{B} that remain masked in state \mathbf{y} . The impact set is defined as

$$S^{\text{impact}}(\mathbf{y}) = \mathcal{M}(\mathbf{y}) \cap S^{\text{high conf}}(\mathbf{y}), \quad (2)$$

where

$$S^{\text{high conf}}(\mathbf{y}) = \left\{ i \in \mathcal{B} \mid \max_{w \in \mathcal{V}} P_{\theta}(y^i = w \mid \mathbf{y}) \geq \tau_{\text{high}} \right\},$$

is the subset of masked indices at which the model is confident enough to form a “visible” future context. For simplic-

ity, we denote the masked set at step t (upon finishing step $t - 1$, prior to finalizing the step- t commit) as

$$\mathcal{M}_t = \{i \in \mathcal{B}_t \mid y_{t-1}^i = [\text{MASK}]\},$$

the high-confidence set at step t as

$$S_t^{\text{high conf}} = \left\{ i \in \mathcal{B}_t \mid \arg \max_{w \in \mathcal{V}} P_{\theta}(y^i = w \mid \mathbf{y}_{t-1}) \geq \tau_{\text{high}} \right\},$$

where \mathcal{B}_t is the current target block. By monitoring S^{impact} as a validity verifier, we enforce consistency under τ_{high} : additional commits must preserve (or expand) the current set of high-confidence future tokens. This metric safeguards decoding, ensuring that bolder commits unlock new information without destabilizing the global trajectory.

At decoding step t , given the committed state \mathbf{y}_{t-1} and the current mask set \mathcal{M}_t , we first identify the **Base Set** $\mathcal{S}_t^{\text{base}} = \mathcal{M}_t \cap S_t^{\text{high conf}}$, i.e., the high-confidence tokens under the model’s default confidence-based parallel decoding.

Committing the tokens in the base set $\mathcal{S}_t^{\text{base}}$ yields the intermediate *base state* $\mathbf{z}_t^{\text{base}}$:

$$\mathbf{z}_t^{i, \text{base}} = \begin{cases} \hat{y}_t^i, & i \in \mathcal{S}_t^{\text{base}} \\ y_{t-1}^i, & i \in [L] \setminus \mathcal{S}_t^{\text{base}} \end{cases} \quad (3)$$

We define the impact set at time t as $\mathcal{S}_t^{\text{impact}} = S^{\text{impact}}(\mathbf{z}_t^{\text{base}})$. Intuitively, the set captures the “future” positions revealed by the commitment of the base set.

4.1. Planning Route Phase I: Planning Proposal

Recent studies indicate that on modern accelerators, inference latency for small batch sizes (e.g., 1 vs. 4) is virtually identical due to memory bandwidth saturation (Wu & Zhang, 2025; Fu et al., 2025). We exploit this parallelism to verify multiple planning candidates simultaneously alongside the baseline trajectory (see Figure 4).

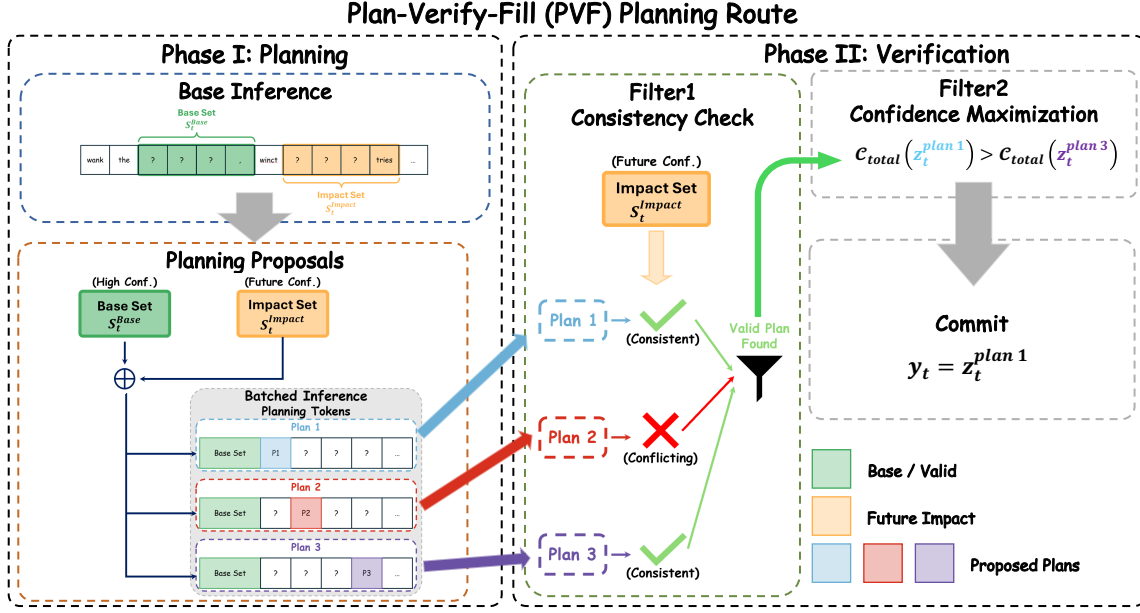


Figure 4. Overview of the Planning Route

Planning Token Candidates Given the vocabulary of planning tokens $\mathcal{P}_{\text{plan}}$, we construct the candidate set $\mathcal{P}_t^{\text{plan}}$ based on $\mathcal{P}_{\text{plan}}$ at step t by identifying masked indices where the model predicts a planning token within the reliable confidence interval $[\tau_{\text{plan}}^l, \tau_{\text{plan}}^u]$. The lower bound τ_{plan}^l acts as a reliability floor, explicitly filtering out low-confidence predictions that would otherwise introduce instability into the generation trajectory. The upper bound τ_{plan}^u serves as an efficiency constraint, excluding tokens that are already approaching convergence (i.e., nearing τ_{high}). Triggering a dedicated planning mechanism in this regime is computationally redundant. Instead, we target the “ambiguous but “promising” interval, tokens where the model exhibits strong intuition but lacks finality, ensuring that the expensive planning budget is allocated strictly to critical decision points where lookahead can significantly clarify the trajectory:

$$\mathcal{P}_t^{\text{plan}} = \left\{ i \in \mathcal{M}_t \mid \hat{y}_t^i \in \mathcal{P}_{\text{plan}} \wedge \tau_{\text{plan}}^l \leq P_{\theta}(y^i = \hat{y}_t^i \mid \mathbf{y}_{t-1}) < \tau_{\text{plan}}^u \right\} \quad (4)$$

We then create an ordered sequence of indices from the candidate set $\mathcal{P}_t^{\text{plan}}$ by sorting them from high to low based on the model P_{θ} ’s confidence. Let $i_{(j)}$ denote the index of the j -th most confident candidate, such that:

$$P_{\theta}(y^{i_{(1)}} = \hat{y}_t^{i_{(1)}} \mid \mathbf{y}_{t-1}) \geq P_{\theta}(y^{i_{(2)}} = \hat{y}_t^{i_{(2)}} \mid \mathbf{y}_{t-1}) \geq \dots \quad (5)$$

where $\hat{y}_t^{i_{(k)}}$ is the predicted token at position $i_{(k)}$. We select the top- k candidates ($j \in [k]$) to construct the planned trajectories

$$z_t^{i, \text{plan } j} = \begin{cases} \hat{y}_t^i, & i = i_j \\ z_t^{i, \text{base}}, & \text{otherwise} \end{cases} \quad (6)$$

Based on a recent paper (Wu et al., 2025b), there is a “free lunch” region where the batch inference costs almost the same computational time as a single sample. Empirically (Fu et al., 2025) demonstrates that on NVIDIA B200, the forward-pass latency for a batch size of 4 is effectively identical to that of a single sample. This configuration allows us to evaluate three planned candidates alongside the single baseline trajectory (a total batch size of 4), maximizing structural exploration without incurring runtime penalty. Finally, if $\mathcal{P}_t^{\text{plan}} = \emptyset$, it indicates that the current context requires local infilling to establish a sufficient foundation before structural planning can resume. In this case, we bypass Phase II and pivot directly to the AR Fallback Route. Conversely, if valid candidates exist but are sparse ($1 \leq |\mathcal{P}_t^{\text{plan}}| < 3$), we continue using all available indices and proceed to Phase II.

4.2. Planning Route Phase II: Verification (The Two-Filter Mechanism)

The design of PVF explicitly distinguishes between *guiding* the model toward coherent structures and *forcing* it into suboptimal commitments. To operationalize this distinction, we employ a two-filter mechanism that rigorously assesses the validity of the planned trajectories generated in Phase I.

Filter 1: Consistency Verification. A planning token is deemed premature if committing to it forces a contradiction in the high-impact future tokens $\mathcal{S}_t^{\text{impact}}$ inferred from the base state. Specifically, for each planned trajectory j , we

verify $\forall i \in \mathcal{S}_t^{\text{impact}}$ if:

$$\arg \max_{w \in \mathcal{V}} P_\theta(y^i = w \mid \mathbf{z}_t^{\text{base}}) = \arg \max_{w \in \mathcal{V}} P_\theta(y^i = w \mid \mathbf{z}_t^{\text{plan } j}) \quad (7)$$

In other words, while the probability distributions over the impact set may fluctuate, the top-1 predictions must remain strictly invariant relative to the Base branch. If a planning token induces a label flip within this high-confidence future region, the candidate trajectory is rejected. This constraint guarantees that introducing planning tokens does not induce behavior inconsistent with the consensus established by the model’s highest-confidence predictions.

Should no candidates satisfy Filter 1, the **PAUSE** mechanism is triggered to prevent cascading errors (i.e. `PAUSE_FLAG` is set to `True`). This failure signal indicates that the proposed planning steps are too aggressive given the current uncertainty and the model lacks sufficient context to reliably establish long-range structure. This mechanism temporarily disables planning, forces a reversion to AR Filling, and commits $\mathbf{y}_t = \mathbf{z}_t^{\text{base}}$ for the current step.

Filter 2: Confidence Maximization. Among the candidates $\mathbf{z}_t^{\text{plan } j}$ that pass Filter 1, we define the *Total Confidence Score* within the current block \mathcal{B}_t :

$$\mathcal{C}_{\text{total}}(\mathbf{z}_t^{\text{plan } j}) = \sum_{i \in \mathcal{B}_t \cap \mathcal{M}(\mathbf{z}_t^{\text{plan } j})} \max_{w \in \mathcal{V}} P_\theta(y^i = w \mid \mathbf{z}_t^{\text{plan } j}) \quad (8)$$

We commit the trajectory $\mathbf{z}_t^{\text{plan } j^*}$ that yields the largest $\mathcal{C}_{\text{total}}$, i.e. $\mathbf{y}_t = \mathbf{z}_t^{\text{plan } j^*}$. Maximizing this metric implies that the selected planning token offers the highest predictive leverage among the considered options, creating the necessary structural conditions for the model to decode the next step with minimal ambiguity.

4.3. AR Fallback Route: Expedited AR Exploration

If the planning route is unavailable or paused, we opt for exploration via AR fallback route to accelerate local content completion before structural planning resumes (see Figure 11). This phase operates as a speculative generation mechanism designed to efficiently fill local content before further structural planning. Unlike classical speculative decoding for AR models, which typically requires training a separate student model (Leviathan et al., 2023), we project this paradigm as a purely inference-time procedure. Additional procedure details are provided in Appendix A.5.1.

5. Experiment Results

5.1. Experiment Settings

We evaluate PVF on six benchmarks datasets spanning mathematical reasoning, coding synthesis, and broad knowledge: GSM8K (Cobbe et al., 2021), MMLU-Pro (Wang et al.,

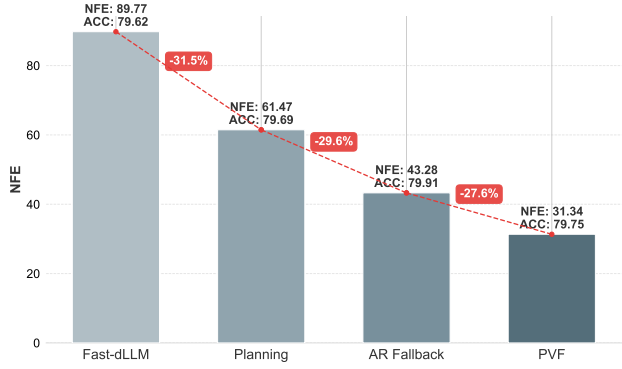


Figure 5. Ablation study on GSM8k, evaluating the contribution of each PVF component. Accuracy scores are displayed in the bracket above each bar to confirm they remain comparable across methods.

2024), ARC-Challenge (ARC-C) (Clark et al., 2018), WinoGrande (Sakaguchi et al., 2021), HumanEval (Chen et al., 2021), and MATH (Hendrycks et al., 2021). LLaDA-8B-Instruct and Dream-7B-Instruct are used as base models to verify that PVF’s performance gains are model-agnostic. We report both accuracy and efficiency, using the Number of Function Evaluations (NFE), the total number of model forward passes required to complete a sequence, as our primary efficiency metric. To ensure a fair comparison, we fix $\tau_{\text{high}} = 0.9$ across all experiments unless stated otherwise. Unless otherwise specified, we follow (Fu et al., 2025; Wu & Zhang, 2025) and use a batch size of 4 ($k = 3$), which lies within the “free lunch” region.

Across all datasets, we use a fixed maximum generation length of $L = 512$ and a block size of $B = 64$. Decoding is training-free (no finetuning, no additional supervision, and no external verifier). Sensitivity to L and B is reported in Section A.4. All experiments are conducted on a single NVIDIA H200 GPU.

Additional experimental details are deferred to section A.6.

5.2. Main Results

Baselines. We benchmark PVF against the static decoding and two training-free acceleration frameworks for DLMs that represent complementary design choices:

- **Static.** A greedy top-1 decoding strategy that commits the most confident token at each iteration.
- **Fast-dLLM (Wu et al., 2025b).** A static confidence-threshold parallel decoding method that commits all tokens whose posterior confidence exceeds τ_{high} .
- **FreeDave (Wu & Zhang, 2025).** A draft-and-verify method that generates multiple look-ahead drafts and commits to the longest consecutively verified span un-

Table 1. Performance comparison with baseline methods. The model name is listed in the leftmost column, with datasets arranged horizontally.

Model	Method	GSM8K		MMLU-Pro		ARC-C		WinoGrande		HumanEval		Math	
		Acc.	NFE	Acc.	NFE	Acc.	NFE	Acc.	NFE	Acc.	NFE	Acc.	NFE
LLaDA-8B	Static	79.46	512.00	36.80	512.00	82.46	512.00	70.24	512.00	46.95	512.00	41.06	512.00
	Fast-dLLM	79.62	89.77	36.20	80.26	83.02	48.75	70.24	48.57	47.56	124.26	40.84	147.16
	Instruct	79.08	135.65	36.70	136.36	84.04	130.73	67.88	131.10	45.73	140.14	40.90	142.82
	PVF	79.62	31.34	36.40	29.55	84.30	17.23	69.93	18.81	46.66	70.31	40.24	73.56
Dream-7B	Static	78.00	512.00	41.30	512.00	86.95	512.00	70.60	512.00	60.37	512.00	42.20	512.00
	Fast-dLLM	77.71	75.83	40.18	92.16	86.78	56.13	70.65	43.01	59.14	112.78	43.46	129.77
	Instruct	79.92	141.01	41.10	91.74	88.23	138.91	69.85	134.10	59.15	112.82	42.00	130.25
	PVF	79.20	32.34	43.30	35.22	87.55	25.93	70.81	16.92	62.66	50.89	43.66	64.80

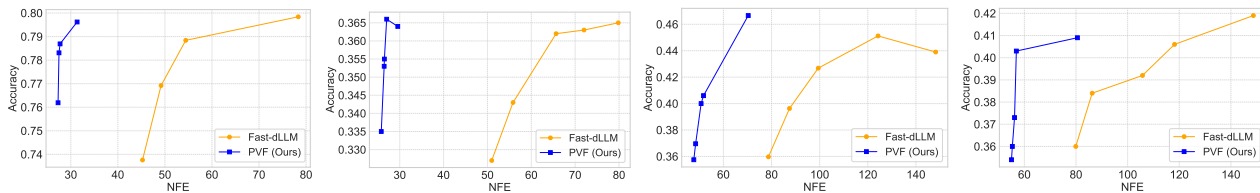


Figure 6. Pareto frontiers for PVF (blue) and Fast-dLLM (orange) on the GSM8K, MMLU-Pro, HumanEval, and Math datasets (from left to right) with LLaDA-8B-Instruct as the base model.

der top-1 decoding, aiming to match the static trajectory with fewer model forward passes.

Comparison. Table 1 summarizes accuracy and NFE across datasets. PVF consistently reduces NFE relative to Fast-dLLM at matched accuracy on all the datasets, while achieving more than 60% fewer forward passes on GSM8K, MMLU-Pro, ARC-C, and WinoGrande, and more than 40% fewer forward passes on MATH and HumanEval. Compared with FreeDave, PVF achieves additional reductions in NFE while maintaining accuracy. Besides, the improvement is consistent across both LLaDa and Dream, indicating the generality of our algorithm. Overall, the results establish PVF as a decoding strategy that delivers substantial efficiency gains while maintaining accuracy.

Figure 6 plots the Pareto frontier (over the evaluated τ_{high} sweep), illustrating the accuracy–efficiency trade-off of PVF versus Fast-dLLM. For a fair comparison, PVF-specific hyperparameters are fixed and only the shared threshold τ_{high} is varied for both methods (see Appendix A.6 for a minor feasibility constraint used on HumanEval and MATH). Note that for MATH, Pareto points are estimated using a 1000-example subset (rather than the full 5000) for computational tractability. PVF consistently dominates Fast-dLLM across operating points. In particular, on GSM8K and MMLU-Pro, near the high-accuracy end of the Pareto frontier, PVF uses less than 50% of the NFE required by Fast-dLLM.

Ablation Study: Contribution of Individual Component
To quantify the efficiency contribution of each component,

we decouple the *planning route* and the *AR fallback route*. In Figure 5, *Planning* isolates the planning route by committing only high-confidence tokens (filtered by τ_{high}) together with the verified lower-confidence planning token identified by the planning route. *AR fallback* commits high-confidence tokens plus additional tokens from the longest verified AR fallback route. As shown in Figure 5, each component alone yields substantial improvements over confidence-based parallel decoding while maintaining accuracy. *AR fallback* tends to be faster per iteration, since it is invoked at every iteration, whereas *Planning* activates only when a suitable planning token is identified. Combining both routes, PVF achieves nearly a 30% improvement over *AR fallback* alone, highlighting the additional efficiency gains provided by the planning mechanism.

6. Conclusion

In this work, we recast the decoding of DLMs not merely as a probabilistic harvesting of tokens, but as a hierarchical process of structural planning. By introducing **PVF**, we demonstrate that the efficiency of parallel generation is unlocked not only by aggressively predicting content, but by stabilizing the *structural skeleton* of the sequence. Our findings reveal that “planning tokens” are pivotal commits that sharply reduce the search space over global trajectories.

Methodologically, PVF contributes a structured, training-free protocol designed to balance aggressive structural commitment with quantitative verification, reducing inference costs significantly while maintaining comparable accuracy.

One potential future direction for DLM decoding is to make the notion of structure more training-aware, so that the model’s representations at inference time better support the same structural decisions PVF makes during decoding. This could better align training and decoding, and may further improve both speed and reliability.

References

- Arriola, M., Gokaslan, A., Chiu, J. T., Yang, Z., Qi, Z., Han, J., Sahoo, S. S., and Kuleshov, V. Block diffusion: Interpolating between autoregressive and diffusion language models. *arXiv preprint arXiv:2503.09573*, 2025.
- Austin, J., Johnson, D. D., Ho, J., Tarlow, D., and Van Den Berg, R. Structured denoising diffusion models in discrete state-spaces. *Advances in neural information processing systems*, 34:17981–17993, 2021.
- Ben-Hamu, H., Gat, I., Severo, D., Nolte, N., and Karrer, B. Accelerated sampling from masked diffusion models via entropy bounded unmasking. *arXiv preprint arXiv:2505.24857*, 2025.
- Berrayana, L., Heakl, A., Sohail, M. A., Hofmann, T., Khan, S., and Chen, W. Planner and executor: Collaboration between discrete diffusion and autoregressive models in reasoning. *arXiv preprint arXiv:2510.15244*, 2025.
- Bogdan, P. C., Macar, U., Nanda, N., and Conmy, A. Thought anchors: Which llm reasoning steps matter? *arXiv preprint arXiv:2506.19143*, 2025.
- Chang, H., Zhang, H., Jiang, L., Liu, C., and Freeman, W. T. Maskgit: Masked generative image transformer. In *Proceedings of the IEEE/CVF conference on computer vision and pattern recognition*, pp. 11315–11325, 2022.
- Chen, B., Martí Monsó, D., Du, Y., Simchowitz, M., Tedrake, R., and Sitzmann, V. Diffusion forcing: Next-token prediction meets full-sequence diffusion. *Advances in Neural Information Processing Systems*, 37:24081–24125, 2024.
- Chen, M., Tworek, J., Jun, H., Yuan, Q., Pinto, H. P. d. O., Kaplan, J., Edwards, H., Burda, Y., Joseph, N., Brockman, G., et al. Evaluating large language models trained on code. *arXiv preprint arXiv:2107.03374*, 2021.
- Chen, Z., Fang, G., Ma, X., Yu, R., and Wang, X. dparallel: Learnable parallel decoding for dllms. *arXiv preprint arXiv:2509.26488*, 2025.
- Cheng, D., Huang, S., Zhu, X., Dai, B., Zhao, W. X., Zhang, Z., and Wei, F. Reasoning with exploration: An entropy perspective. *arXiv preprint arXiv:2506.14758*, 2025.
- Clark, P., Cowhey, I., Etzioni, O., Khot, T., Sabharwal, A., Schoenick, C., and Tafjord, O. Think you have solved question answering? try arc, the ai2 reasoning challenge. *arXiv preprint arXiv:1803.05457*, 2018.
- Cobbe, K., Kosaraju, V., Bavarian, M., Chen, M., Jun, H., Kaiser, L., Plappert, M., Tworek, J., Hilton, J., Nakano, R., et al. Training verifiers to solve math word problems. *arXiv preprint arXiv:2110.14168*, 2021.

- Fu, H., Huang, B., Adams, V., Wang, C., Srinivasan, V., and Jiao, J. From bits to rounds: Parallel decoding with exploration for diffusion language models. *arXiv preprint arXiv:2511.21103*, 2025.
- Gong, S., Agarwal, S., Zhang, Y., Ye, J., Zheng, L., Li, M., An, C., Zhao, P., Bi, W., Han, J., et al. Scaling diffusion language models via adaptation from autoregressive models. *arXiv preprint arXiv:2410.17891*, 2024.
- Google DeepMind. Gemini diffusion, 2025. URL <https://deepmind.google/models/gemini-diffusion/>. Accessed: 2025.
- Hendrycks, D., Burns, C., Kadavath, S., Arora, A., Basart, S., Tang, E., Song, D., and Steinhardt, J. Measuring mathematical problem solving with the math dataset. *arXiv preprint arXiv:2103.03874*, 2021.
- Hoogeboom, E., Gritsenko, A. A., Bastings, J., Poole, B., Berg, R. v. d., and Salimans, T. Autoregressive diffusion models. *arXiv preprint arXiv:2110.02037*, 2021.
- Huang, P., Liu, S., Liu, Z., Yan, Y., Wang, S., Chen, Z., and Xiao, T. Pc-sampler: Position-aware calibration of decoding bias in masked diffusion models. *arXiv preprint arXiv:2508.13021*, 2025.
- Israel, D., Jin, T., Cheng, E., Broeck, G. V. d., Grover, A., Subramanian, S., and Carbin, M. Planned diffusion. *arXiv preprint arXiv:2510.18087*, 2025.
- Jin, X., Wang, Y., Gao, Y., Wen, Z., Qi, B., Liu, D., and Zhang, L. Thinking inside the mask: In-place prompting in diffusion llms. *arXiv preprint arXiv:2508.10736*, 2025.
- Khanna, S., Kharbanda, S., Li, S., Varma, H., Wang, E., Birnbaum, S., Luo, Z., Miraoui, Y., Palrecha, A., Ermon, S., et al. Mercury: Ultra-fast language models based on diffusion. *arXiv preprint arXiv:2506.17298*, 1, 2025.
- Leviathan, Y., Kalman, M., and Matias, Y. Fast inference from transformers via speculative decoding. In *International Conference on Machine Learning*, pp. 19274–19286. PMLR, 2023.
- Li, J.-N., Guan, J., Wu, W., and Li, C. Refusion: A diffusion large language model with parallel autoregressive decoding. *arXiv preprint arXiv:2512.13586*, 2025a.
- Li, X., Thickstun, J., Gulrajani, I., Liang, P. S., and Hashimoto, T. B. Diffusion-lm improves controllable text generation. *Advances in neural information processing systems*, 35:4328–4343, 2022.
- Li, Y., Dong, Z., Sun, Y., Wang, W., Xiong, S., Luo, Y., Liu, J., Lu, H., Wang, J., Su, W., et al. Attention illuminates llm reasoning: The preplan-and-anchor rhythm enables fine-grained policy optimization. *arXiv preprint arXiv:2510.13554*, 2025b.
- Lou, A., Meng, C., and Ermon, S. Discrete diffusion language modeling by estimating the ratios of the data distribution. 2023.
- Lou, A., Meng, C., and Ermon, S. Discrete diffusion modeling by estimating the ratios of the data distribution. In *Proceedings of the 41st International Conference on Machine Learning*, pp. 32819–32848, 2024.
- Nie, S., Zhu, F., You, Z., Zhang, X., Ou, J., Hu, J., Zhou, J., Lin, Y., Wen, J.-R., and Li, C. Large language diffusion models. *arXiv preprint arXiv:2502.09992*, 2025.
- Ou, J., Nie, S., Xue, K., Zhu, F., Sun, J., Li, Z., and Li, C. Your absorbing discrete diffusion secretly models the conditional distributions of clean data. *arXiv preprint arXiv:2406.03736*, 2024.
- Prabhudesai, M., Wu, M., Zadeh, A., Fragkiadaki, K., and Pathak, D. Diffusion beats autoregressive in data-constrained settings. *arXiv preprint arXiv:2507.15857*, 2025.
- Sahoo, S., Arriola, M., Schiff, Y., Gokaslan, A., Marroquin, E., Chiu, J., Rush, A., and Kuleshov, V. Simple and effective masked diffusion language models. *Advances in Neural Information Processing Systems*, 37:130136–130184, 2024.
- Sakaguchi, K., Bras, R. L., Bhagavatula, C., and Choi, Y. Winogrande: An adversarial winograd schema challenge at scale. *Communications of the ACM*, 64(9):99–106, 2021.
- Shi, J., Han, K., Wang, Z., Doucet, A., and Titsias, M. Simplified and generalized masked diffusion for discrete data. *Advances in neural information processing systems*, 37:103131–103167, 2024.
- Wang, S., Yu, L., Gao, C., Zheng, C., Liu, S., Lu, R., Dang, K., Chen, X., Yang, J., Zhang, Z., et al. Beyond the 80/20 rule: High-entropy minority tokens drive effective reinforcement learning for llm reasoning. *arXiv preprint arXiv:2506.01939*, 2025a.
- Wang, X., Caccia, L., Ostapenko, O., Yuan, X., Wang, W. Y., and Sordoni, A. Guiding language model reasoning with planning tokens. *arXiv preprint arXiv:2310.05707*, 2023.
- Wang, X., Xu, C., Jin, Y., Jin, J., Zhang, H., and Deng, Z. Diffusion llms can do faster-than-ar inference via discrete diffusion forcing. *arXiv preprint arXiv:2508.09192*, 2025b.

- Wang, Y., Ma, X., Zhang, G., Ni, Y., Chandra, A., Guo, S., Ren, W., Arulraj, A., He, X., Jiang, Z., et al. Mmlu-pro: A more robust and challenging multi-task language understanding benchmark. *arXiv preprint arXiv:2406.01574*, 2024.
- Wu, C., Zhang, H., Xue, S., Diao, S., Fu, Y., Liu, Z., Molchanov, P., Luo, P., Han, S., and Xie, E. Fast-dllm v2: Efficient block-diffusion llm. *arXiv preprint arXiv:2509.26328*, 2025a.
- Wu, C., Zhang, H., Xue, S., Liu, Z., Diao, S., Zhu, L., Luo, P., Han, S., and Xie, E. Fast-dllm: Training-free acceleration of diffusion llm by enabling kv cache and parallel decoding. *arXiv preprint arXiv:2505.22618*, 2025b.
- Wu, S. and Zhang, J. Free draft-and-verification: Toward lossless parallel decoding for diffusion large language models. *arXiv preprint arXiv:2510.00294*, 2025.
- Yang, Y., Wang, C., Wang, S., Wen, Z., Qi, B., Xu, H., and Zhang, L. Diffusion llm with native variable generation lengths: Let [eos] lead the way. *arXiv preprint arXiv:2510.24605*, 2025.
- Ye, J., Xie, Z., Zheng, L., Gao, J., Wu, Z., Jiang, X., Li, Z., and Kong, L. Dream 7b: Diffusion large language models. *arXiv preprint arXiv:2508.15487*, 2025a.
- Ye, Z., Zhang, Z., Zhang, Y., Ma, J., Lin, J., and Feng, F. Disentangling reasoning tokens and boilerplate tokens for language model fine-tuning. In *Findings of the Association for Computational Linguistics: ACL 2025*, pp. 20939–20957, 2025b.
- Yu, R., Ma, X., and Wang, X. Dimple: Discrete diffusion multimodal large language model with parallel decoding. *arXiv preprint arXiv:2505.16990*, 2025.
- Zhang, M., Wang, Z., Yang, Z., Feng, W., and Lan, A. Interpretable math word problem solution generation via step-by-step planning. *arXiv preprint arXiv:2306.00784*, 2023.
- Zhou, C., Wang, C., Zhang, D., Tong, S., Wang, Y., Bates, S., and Jaakkola, T. Next semantic scale prediction via hierarchical diffusion language models. *arXiv preprint arXiv:2510.08632*, 2025.
- Zhu, F., Wang, R., Nie, S., Zhang, X., Wu, C., Hu, J., Zhou, J., Chen, J., Lin, Y., Wen, J.-R., et al. Llada 1.5: Variance-reduced preference optimization for large language diffusion models. *arXiv preprint arXiv:2505.19223*, 2025.

A. Appendix

A.1. Planning Tokens

This section delineates the methodology for constructing the set of planning tokens \mathcal{P} —a vocabulary of high-frequency syntactic and semantic anchors that govern the structural trajectory of the generated sequence. To ensure both coverage and precision, our construction methodology employs a hybrid strategy that integrates *static structural distillation* with the *deterministic discourse anchoring* described below.

Static List Acquisition via Structural Distillation Manually curating a comprehensive planning vocabulary is intractable given the diversity of generation contexts. To address this, we utilize a modern Large Language Model (e.g., Gemini 3 Pro) as a *structural distillation engine* to extract a compact, domain-invariant set of tokens. We enforce strict constraints to ensure the generated tokens are content-neutral and syntax-safe, explicitly excluding invisible control characters and variable-specific identifiers. The prompt template used to generate this list is shown below, followed by the static token list returned by Gemini 3 Pro. Notably, the generated static list also includes common reasoning and mathematical operator anchors (e.g., +, −), consistent with prior work that studies such markers as planning signals for improved reasoning behavior (Zhang et al., 2023).

Prompt: Generating Planning Tokens

I need a “Planning Token” list for a parallel decoding algorithm of diffusion language models. These tokens act as the structural skeleton of valid code/text. **The Rules (Strict Adherence Required):**

1. **Content Neutrality:** The list must **ONLY** contain language primitives (keywords, operators, built-ins, standard delimiters). Do **NOT** include variable names (e.g., `i`, `x`, `data`), common string literals, or domain-specific business logic words.
2. **Syntax Safety:** **EXCLUDE** all invisible formatting or whitespace tokens. Specifically, **NO** newlines (`\n`), tabs (`\t`), carriage returns (`\r`), or solitary whitespace tokens. Every token must be a visible, functional anchor.
3. **High Frequency:** These must be the most ubiquitous tokens in the language, required for almost any valid file.

Anchoring Logical Pivots via Sentence-Initial Tokens In addition, note that in multi-step reasoning domains, specific discourse markers—such as *Therefore*, *Thus*, *However*, or *Step 1*—serve as high-leverage **logical pivots**. These tokens explicitly delimit the structural boundary between a preceding premise and a new deduction. To comprehensively capture these influential anchors without relying on an exhaustive manual list, we implement a deterministic syntactic prior that targets the superset of these markers: all *capitalized initial tokens*. Since capitalization predominantly signals the **sentence-initial position**, this criterion robustly identifies the structural onsets of new reasoning blocks. By treating these sentence starters as planning tokens, our method enforces a **structural lock**, ensuring the model commits to the causal trajectory of the next logical step before generating the dependent semantic content. This is consistent with prior work highlighting discourse cues as structural anchors in multi-step reasoning (Wang et al., 2025a).

Anchoring the Termination Boundary Complementing the initiation anchors, we explicitly designate the End-of-Sequence (EOS) token as the definitive **terminal anchor**. In the context of diffusion decoding, the EOS token functions not merely as a cessation signal, but as a critical structural scaffold that delimits the finite boundary of the generation trajectory (Yang et al., 2025). By treating termination as a high-priority planning event, our algorithm acts to **preemptively truncate** the decoding process the instant the logical conclusion is realized. This ensures that the generation trajectory is rigorously bounded, preventing computational expenditure on post-conclusion noise and enforcing a precise structural endpoint to the chain of thought.

Planning Token Reference List

1. Control Flow & Structure (The Skeleton)

def, class, return, import, from, as, if, elif, else, for, while, break, continue, pass, try, except, raise, finally, with, assert, lambda, yield, global, nonlocal, del

2. Logical & Comparison Operators (The Decision Makers)

and, or, not, is, in, ==, !=, >=, <=, >, <

3. Critical Punctuation (The Syntax Glue)

:, (,), [,], {, }, ,, ., -, @

4. Built-in Functions (Action Anchors)

len, range, enumerate, zip, sorted, reversed, int, float, str, list, dict, set, tuple, bool, sum, max, min, abs, round, pow, divmod, print, input, open, map, filter, all, any, isinstance, subclass, type

5. Common Methods (Data Structure Anchors)

append, extend, insert, remove, pop, clear, index, count, sort, reverse, get, keys, values, items, update, add, union, intersection, difference, split, join, strip, replace, format, startswith, endswith, lower, upper

6. Reasoning, Math, & Comment Anchors

#, =, +, -, *, /, //, %, **, +=, -=, *=, /=

7. Dynamic & Special Anchors (Context-Aware)

- **End of Text Token (EOS):** (<|endoftext|>)
- **Capitalized Initial Words:** Any token starting with a capital letter (e.g., Therefore, If, Let).

A.2. Additional Details of Ablation Studies

Ablation setting (Section 3). We evaluate two exploration variants—*Random* and *Planning*—under the same Semi-Autoregressive Blockwise Decoding framework introduced in Section 2. At each decoding iteration, we proceed as follows.

1. **High-confidence commits.** We first commit all masked positions that satisfy the static Fast-dLLM unmasking rule (Wu et al., 2025b) with threshold $\tau_{\text{high}} = 0.9$.
2. **Low-confidence exploration within a confidence bin.** Let $[\tau^l, \tau^u]$ denote the active confidence range (bin). Among the remaining masked positions in the current active block whose top-1 posterior confidence lies in $[\tau^l, \tau^u]$, we commit exactly one additional token using one of the following strategies:
 - (a) **Random.** Uniformly sample one eligible masked position (within the block) and commit its top-1 token.
 - (b) **Planning.** We form the subset of eligible masked positions whose top-1 token is in \mathcal{P} and whose confidence lies in $[\tau^l, \tau^u]$. If this subset is non-empty, we uniformly sample one element from it and commit its top-1 token. If it is empty, we fall back to the same Random rule above (sampling from all eligible positions in $[\tau^l, \tau^u]$).

The fallback in the Planning variant is important for a fair comparison: since \mathcal{P} is deliberately small, the planning-eligible subset is sometimes empty (see Figure 9). Without a fallback, the Planning variant would make fewer low-confidence commits, confounding accuracy and runtime with a different number of exploration steps. By enforcing a matched exploration rate via fallback, improvements can be attributed to *which* low-confidence tokens are committed (semantic/structural anchors) rather than *how many* are committed.

Additionally, Table A.2 reports the average confidence of the extra lower-confidence tokens committed under both the **Random** and **Planning** strategies. Across all datasets, the average values differ by at most 0.01, indicating that the gains in efficiency and accuracy are driven by prioritizing commits to planning tokens, rather than due to a statistical bias whereby planning tokens exhibit systematically higher posterior confidence within the same confidence band.

Speedup metric. We quantify decoding speed by the number of function evaluations (NFE), i.e., the total number of forward passes. For each setting, we report speedup as

$$\text{Speedup} = \frac{\text{NFE}_{\text{Fast-dLLM}}}{\text{NFE}_{(\text{Random/Planning})}},$$

so that larger values indicate fewer forward passes and faster decoding.

Table 2. Comparison of Planning versus Random token strategies in low-confidence regimes. The average confidence (*Avg Token Conf*) of the selected tokens is maintained at comparable levels to ensure a controlled comparison.

Dataset	τ^l	τ^u	Method	Acc.	NFE	Avg. Token Conf.
GSM8K	0.10	0.60	Planning	0.73	50.67	0.38
			Random	0.70	53.97	0.38
	0.15	0.60	Planning	0.74	49.63	0.40
			Random	0.71	51.97	0.39
	0.20	0.60	Planning	0.75	49.78	0.42
			Random	0.72	52.04	0.41
	0.25	0.60	Planning	0.76	50.55	0.43
			Random	0.74	51.89	0.44
HumanEval	0.10	0.60	Planning	0.24	66.38	0.37
			Random	0.18	78.57	0.36
	0.15	0.60	Planning	0.31	67.54	0.39
			Random	0.24	68.74	0.38
	0.20	0.60	Planning	0.30	66.99	0.41
			Random	0.24	70.87	0.40
	0.25	0.60	Planning	0.30	68.90	0.43
			Random	0.26	70.39	0.43

A.3. Additional Experiments

A.3.1. SENSITIVITY ANALYSIS: GENERATION LENGTH AND BLOCK SIZE

To evaluate the robustness of our approach, we benchmark PVF against the Fast-dLLM baseline across varying maximum generation lengths ($L \in \{256, 512\}$) and block sizes ($k \in \{16, 32, 64\}$) on the GSM8K dataset. As shown in Table 3, PVF consistently demonstrates a substantial improvement in algorithmic efficiency, achieving significantly lower NFE than Fast-dLLM across all configurations while maintaining near-identical accuracy. Furthermore, we observe a positive correlation between block size and efficiency gains: as the block size increases, the reduction in NFE becomes more pronounced. This trend validates the efficacy of our planning mechanism, which leverages larger blocks to secure longer verified decoding trajectories, thereby minimizing the number of required forward passes more effectively.

Table 3. Comparison of PVF and Fast-dLLM performance across different Generation Lengths and Block Sizes on GSM8K for LLaDA-8B-Instruct.

Gen Length	Block Size	PVF		Fast-dLLM	
		Accuracy	NFE	Accuracy	NFE
256	16	76.46	37.76	76.30	77.73
	32	75.92	26.75	75.76	71.23
	64	75.84	24.52	75.69	67.85
512	16	79.53	58.34	80.07	110.32
	32	79.92	41.55	79.69	96.86
	64	79.62	31.34	79.62	89.77

A.3.2. SENSITIVITY ANALYSIS: PLANNING TOKEN THRESHOLDS $\tau_{\text{PLAN}}^l, \tau_{\text{PLAN}}^u$

We further investigate the sensitivity of PVF to the planning-token thresholds, specifically the lower bound τ_{plan}^l and upper bound τ_{plan}^u . To ensure a fair comparison, we fix all other hyperparameters to match those used in Table 1 for both datasets.

Across the range of values we test, accuracy remains largely stable, indicating that the planning-token procedure is reasonably reliable. We nonetheless observe a mild trade-off between algorithmic efficiency and generation quality: lowering both threshold bounds consistently reduces NFE (improving efficiency) but leads to a corresponding minor decline in accuracy. This behavior occurs because lowering the thresholds effectively forces the model to commit to planning tokens with lower confidence. While this aggressive commitment typically provides a stronger contextual signal that boosts the confidence of subsequent tokens, which accelerates the decoding process, it simultaneously increases the chance of making mistakes.

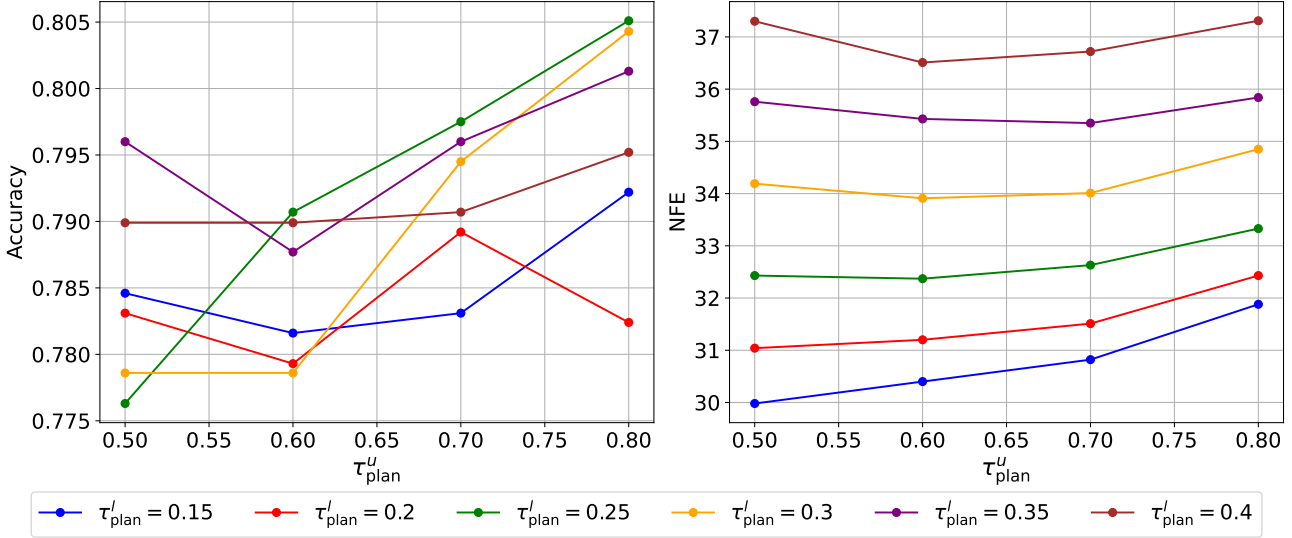


Figure 7. Sensitivity analysis of planning-token thresholds on GSM8K. Each curve corresponds to a fixed lower bound τ_{plan}^l and shows accuracy and NFE as τ_{plan}^u varies.

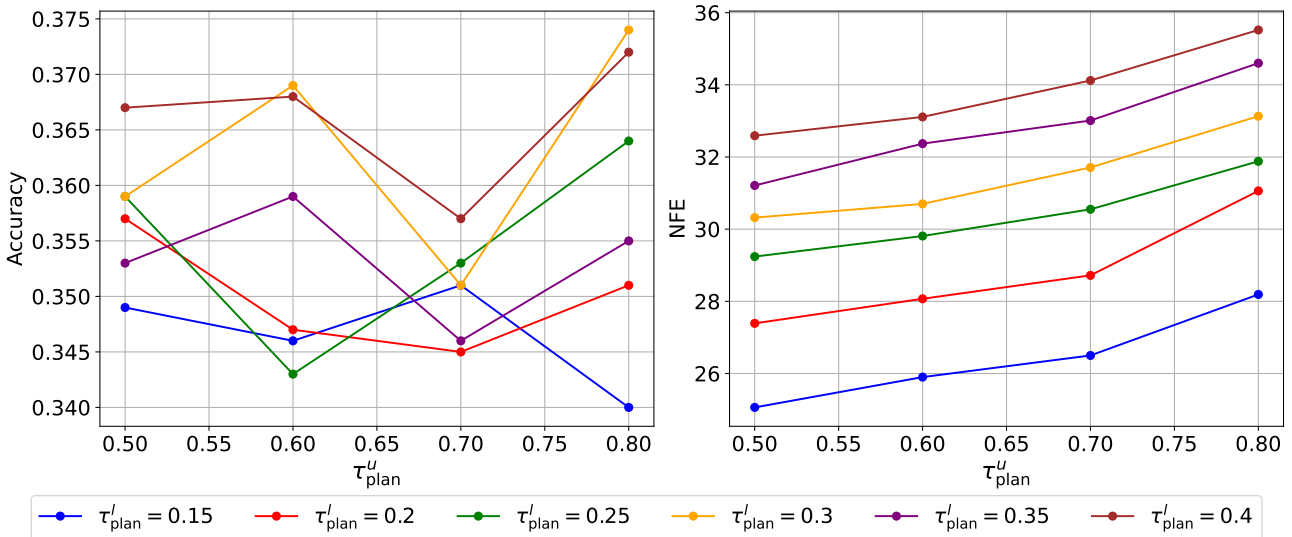


Figure 8. Sensitivity analysis of planning-token thresholds on MMLU-Pro. Each curve corresponds to a fixed lower bound τ_{plan}^l and shows accuracy and NFE as τ_{plan}^u varies.

We further examine the percentage of planning tokens relative to the total token count (defined as the sum of planning and AR fallback tokens) under varying lower bound thresholds τ_{plan}^l , while fixing the upper bound at $\tau_{\text{plan}}^u = 0.9$. Figure 9 illustrates this relationship, showing that a lower threshold results in a higher proportion of selected planning tokens, which in turn typically leads to better algorithmic efficiency.

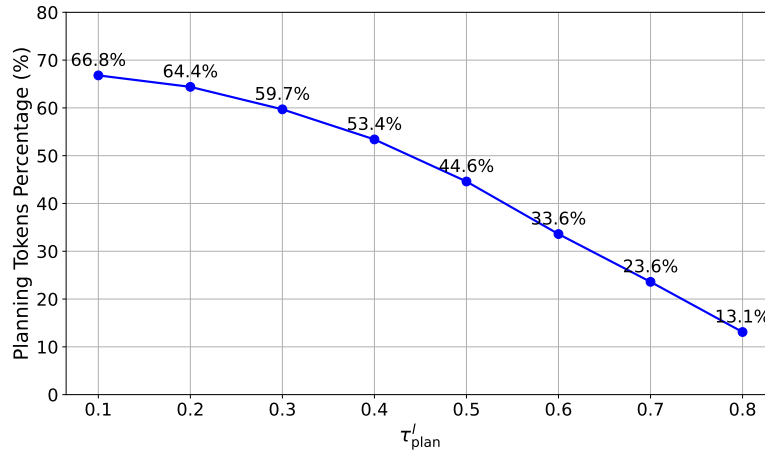


Figure 9. Impact of the planning token threshold lower bound (τ_{plan}^l) on the percentage of selected planning tokens.

A.4. Ablation Study: Sensitivity to Batch Size

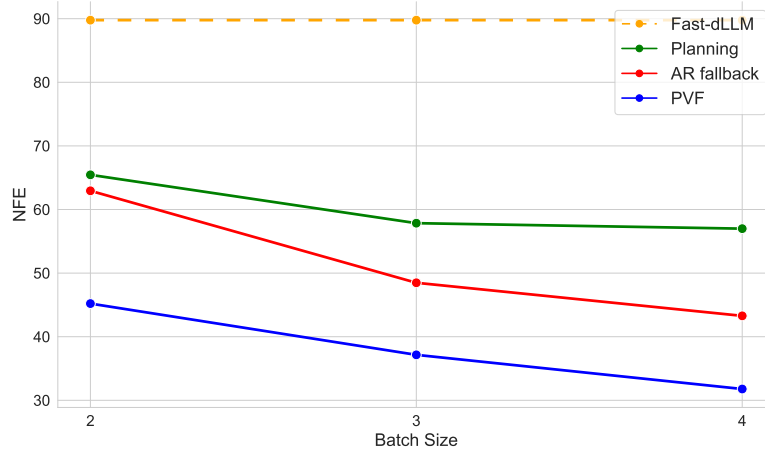


Figure 10. Ablation study on the full GSM8k dataset evaluating the impact of PVF components across varying batch sizes in the “free lunch” regime. All results maintain lossless accuracy compared to static decoding.

To assess whether our algorithm retains efficiency even with more constrained batch sizes, we evaluate the NFE of our PVF method and its individual components as the batch size varies, ensuring that accuracy remains lossless relative to static decoding. In Figure 10, we observe that the planning stage delivers stable performance even at a batch size of 2, whereas the AR fallback benefits more significantly from larger batches due to its cumulative nature. Notably, the full PVF method consistently outperforms both individual components across all settings, and demonstrates substantial efficiency gains compared to the baseline method even at a batch size of 2.

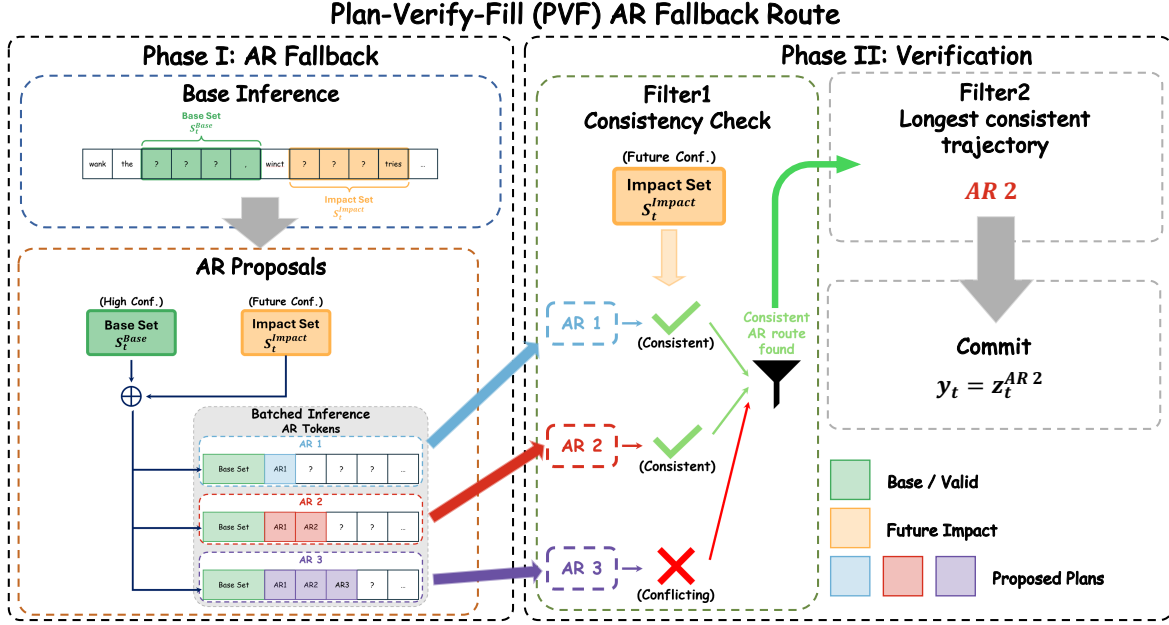


Figure 11. Overview of the AR Fallback Route

A.5. Additional Details of PVF

A.5.1. AR FALLBACK ROUTE

In this section, we introduce how AR routes are constructed and selected.

Candidate Construction. A batch of candidate trajectories is constructed by tentatively fixing the k -leftmost masked tokens (for $k = 1, 2, 3$) whose confidence (defined as $\max_{w \in \mathcal{V}} P_\theta(y^i = w | \mathbf{y})$) is larger than a threshold τ_{AR}^l from the set $\mathcal{M}_t \setminus S_t^{\text{base}}$. Let these indices be denoted as $\{i_1^{\text{AR}}, i_2^{\text{AR}}, i_3^{\text{AR}}\}$ in ascending order. The AR candidate trajectories $\mathbf{z}_t^{\text{AR } k}$ are defined as follows:

$$z_t^{i, \text{AR } k} = \begin{cases} \hat{y}_t^i, & i \in \{i_1^{\text{AR}}, \dots, i_k^{\text{AR}}\} \\ z_t^{i, \text{base}}, & \text{otherwise} \end{cases} \quad (9)$$

AR Verification. To ensure generation quality, we design a rigorous verification process. We accept a k -token extension only if the model's predictions on the new trajectory are *consistent* with the tentative drafts. Formally, for a candidate k , we verify:

$$\forall i \in \{i_1^{\text{AR}}, \dots, i_k^{\text{AR}}\}, \quad \operatorname{argmax}_{w \in \mathcal{V}} P_\theta(y^i = w | \mathbf{z}_t^{\text{base}}) = z_t^{i, \text{AR } k} \quad (10)$$

Let k^* denote the largest k satisfying the verification condition (10). We commit the corresponding trajectory $\mathbf{y}_t = \mathbf{z}_t^{\text{AR } k^*}$. This constraint ensures that the AR fallback only accepts tokens that remain stable under the updated context, effectively mitigating hallucinations.

In the event that no candidate passes verification, the system reverts to the base state $\mathbf{y}_t = \mathbf{z}_t^{\text{base}}$. Upon entering the AR fallback phase, the PAUSE_FLAG is reset to False. This ensures the suspension of planning is transient, encouraging the model to re-attempt structural planning in subsequent steps once the local context has been stabilized.

A.5.2. PLANNING-GUIDED EARLY CROSS-BLOCK REVELATION

While retaining block-wise efficiency, PVF discards the rigid requirement of strictly sequential convergence. Our motivation is structural: as the active block enters a *saturated regime* of mask scarcity, the constricted search space limits the planner's

optimization capacity. To counteract this, we adopt a *dynamic expansion strategy* that reveals the subsequent block preemptively when the current block’s sparsity hinders effective planning.

Consistent with recent approaches that relax rigid block boundaries (Wang et al., 2025b; Fu et al., 2025), we allow for early cross-block revelation to facilitate information flow. However, to mitigate the accuracy degradation often observed with aggressive expansion (Wang et al., 2025b), this strategy is implemented conservatively. Expansion is only triggered when the current block enters a saturated regime of mask scarcity, ensuring that the early decoding mechanism serves solely to maintain a valid planning horizon.

Formally, the block size is denoted as $S = L/B$. We identify the index of the current active block k_t as the first block containing masked tokens. Define the index set of masked tokens in the current active block $\mathcal{M}_t^{\text{active}} = \{i | y_{t-1}^i = [\text{MASK}]\} \cap \{S(k_t - 1) + 1, \dots, Sk_t\}$. We define the working index set \mathcal{B}_t by checking if the remaining masks in the current block fall below a sparsity threshold N_s :

$$\mathcal{B}_t = \begin{cases} \mathcal{M}_t^{\text{active}} \cup \mathcal{I}_{k_t+1}, & \text{if } |\mathcal{M}_t^{\text{active}}| \leq N_s \\ \mathcal{M}_t^{\text{active}}, & \text{otherwise} \end{cases} \quad (11)$$

where $\mathcal{I}_{k_t+1} = \{k_t S + 1, \dots, (k_t + 1)S\}$ represents the full index range of the next block. This condition ensures that the planner always operates on a sufficiently broad horizon, seamlessly transitioning focus to $k + 1$ as block k_t stabilizes.

Algorithm 1 Plan-Verify-Fill (PVF) Decoding

```

1: Input: Model  $P_\theta$ , Sequence Length  $L$ , Thresholds  $\tau_{\text{high}}, \tau_{\text{plan}}$ 
2: Initialize:  $\mathbf{y}_0 \leftarrow [\text{MASK}]^L, t \leftarrow 0$ 
3: while  $\mathbf{y}_t$  contains [MASK] do
4:   Route Selection:
5:     Identify planning candidates  $\mathcal{P}_t^{\text{plan}}$  (tokens with sufficient confidence)
6:     if  $\mathcal{P}_t^{\text{plan}} \neq \emptyset$  and PAUSE_FLAG is False then
7:       Choose the Planning Route
8:     else
9:       Choose the AR Fallback Route
10:    end if
11:  Planning Route:
12:    Construct up to 3 candidate trajectories  $\mathbf{z}_t^{\text{plan } 1}, \mathbf{z}_t^{\text{plan } 2}, \mathbf{z}_t^{\text{plan } 3}$ , according to (6). Run parallel forward pass:
13:     $P_\theta \left( \{ \mathbf{z}_t^{\text{base}}, \mathbf{z}_t^{\text{plan } 1}, \mathbf{z}_t^{\text{plan } 2}, \mathbf{z}_t^{\text{plan } 3} \} \mid \mathbf{y}_{t-1} \right)$ 
14:    Filter 1: Identify planning trajectories that are consistent with Base on  $S_t^{\text{impact}}$  by (7).
15:    if there does not exist a non-contradictory planning trajectory:
16:      Commit  $\mathbf{y}_t = \{ \mathbf{z}_t^{\text{base}} \}$ , and set the PAUSE_FLAG as True, and skip Filter 2.
17:    else
18:      Proceed to Filter 2 below.
19:    end if
20:    Filter 2: Select  $j^*$  among the consistent trajectories that maximizes  $\mathcal{C}_{\text{total}}$ , defined in (8). Commit  $\mathbf{y}_t = \mathbf{z}_t^{\text{plan } j^*}$ .
21:     $t \leftarrow t + 1$ .
22:  Continue
23:  AR Fallback Route:
24:    Construct AR fallback trajectories  $\mathbf{z}_t^{\text{AR } 1}, \mathbf{z}_t^{\text{AR } 2}, \mathbf{z}_t^{\text{AR } 3}$  as defined in (9).
25:    Check consistency with base trajectory  $\mathbf{z}_t^{\text{base}}$  as described in (10).
26:    if there does not exist a non-contradictory planning trajectory,
27:      Commit  $\mathbf{y}_t \leftarrow \mathbf{z}_t^{\text{base}}$ .
28:    else
29:      Select largest  $k$  that  $\mathbf{z}_t^{\text{AR } k}$  is consistent with  $\mathbf{z}_t^{\text{base}}$ , and denote it as  $\mathbf{z}_t^{\text{AR } k^*}$ . Then commit  $\mathbf{y}_t \leftarrow \mathbf{z}_t^{\text{AR } k^*}$ .
30:    end if
31:     $t \leftarrow t + 1$ , set PAUSE_FLAG to False
32: end while
33: Return  $\mathbf{y}$ 

```

A.6. Additional Experimental Details

Experimental details. Across all datasets, we use a fixed maximum generation length of $L = 512$ and a block size of $B = 64$. Decoding is training-free (no finetuning, no additional supervision, and no external verifier). All experiments are conducted on a single NVIDIA H200 GPU.

Implementation and evaluation. All methods share the same prompt templates per dataset, the same stopping criterion, and the same maximum generation length. For HumanEval, we follow the standard unit-test protocol and report pass@1. For MATH and GSM8K, we use exact-match evaluation on the final answer. For MMLU-Pro, ARC-C, and WinoGrande, we report multiple-choice accuracy.

Hyper-parameters. Table 4 summarizes the hyperparameters used across benchmarks.

Benchmark	Base Budget (L, B)	Planning Thresholds ($\tau_{\text{plan}}^l, \tau_{\text{plan}}^u$)	AR Fallback Threshold τ_{AR}^l	Early Cross-block Threshold N_s
MMLU-Pro	$L=512, B=64$	(0.2, 0.65)	0.1	5
ARC-C	$L=512, B=64$	(0.2, 0.65)	0.1	5
WinoGrande	$L=512, B=64$	(0.2, 0.65)	0.1	5
GSM8K	$L=512, B=64$	(0.2, 0.65)	0.1	5
HumanEval	$L=512, B=64$	(0.8, 0.9)	0.5	0
MATH	$L=512, B=64$	(0.8, 0.9)	0.35	0

Table 4. Report of Hyperparameters Used

For the Pareto sweeps in Fig. 6 on HumanEval and MATH, we additionally enforce a feasibility constraint that the planning range does not overlap with the high-confidence region $(\tau_{\text{high}}, 1)$, since overlapping these zones would make the roles of “planning” versus “high-confidence” commits ill-defined. Concretely, we set $(\tau_{\text{plan}}^l, \tau_{\text{plan}}^u) = (0.4, 0.6)$ for $\tau_{\text{high}} < 0.9$.

A.7. Case study

In this section, we present two example generations from LLaDA-8B-Instruct using Fast-dLLM and our PVF strategy. For PVF, we highlight tokens committed via the planning route in yellow and tokens committed via the AR fallback route in pink.

LLaDA Prediction of Fast-dLLM (89 steps)

To determine the total number of hours Meredith spent writing articles over the three days, we need to follow these steps:

1. Calculate the number of articles she wrote on Tuesday.
2. Calculate the number of articles she wrote on Wednesday.
3. Find the total number of articles she wrote over the three days.
4. Calculate the total number of hours she spent writing the articles.

****Step 1: Calculate the number of articles she wrote on Tuesday.****

Meredith wrote 5 articles on Monday. On Tuesday, she wrote $\left(\frac{2}{5}\right)$ times more articles than on Monday. Therefore, the number of articles she wrote on Tuesday is:

$$\left[\begin{array}{l} 5 + \frac{2}{5} \times 5 = 5 + 2 = 7 \\ \end{array} \right]$$

****Step 2: Calculate the number of articles she wrote on Wednesday.****

On Wednesday, she wrote twice the number of articles she wrote on Tuesday. Therefore, the number of articles she wrote on Wednesday is:

$$\left[\begin{array}{l} 2 \times 7 = 14 \\ \end{array} \right]$$

****Step 3: Find the total number of articles she wrote over the three days.****

The total number of articles she wrote over the three days is the sum of the articles she wrote on Monday, Tuesday, and Wednesday:

$$\left[\begin{array}{l} 5 + 7 + 14 = 26 \\ \end{array} \right]$$

****Step 4: Calculate the total number of hours she spent writing the articles.****

Each article takes an average of 4 hours to research and write. Therefore, the total number of hours she spent writing the articles is:

$$\left[\begin{array}{l} 26 \times 4 = 104 \\ \end{array} \right]$$

Thus, the total number of hours she spent writing articles in the three days is $\boxed{104}$.

LLaDA Prediction with PVF (36 steps)

To determine the total number of hours Meredith spent writing articles over the three days, we need to follow these steps:

1. Calculate the number of articles she wrote on Tuesday.
2. Calculate the number of articles she wrote on Wednesday.
3. Find the total number of articles written each day.
4. Calculate the total number of hours spent writing over the three days.

Step 1: Calculate the number of articles written on Tuesday.

Meredith wrote 5 articles on Monday. On Tuesday, she wrote $\left(\frac{2}{5}\right)$ times more articles than on Monday. Therefore, the number of articles written on Tuesday is:

$$5 + \frac{2}{5} \times 5 = 5 + 2 = 5 + 2 = 7$$

Step 2: Calculate the number of articles written on Wednesday.

On Wednesday, she wrote twice the number of articles she wrote on Tuesday. Therefore, the number of articles written on Wednesday is:

$$2 \times 7 = 14$$

Step 3: Find the total number of articles written each day.

- On Monday, she wrote 5 articles.
- On Tuesday, she wrote 7 articles.
- On Wednesday, she wrote 14 articles.

Step 4: Calculate the total number of hours spent writing over the three days.

Each article takes an average of 4 hours to research and write. Therefore, the total number of hours spent writing each day is:

- On Monday: $(5 \text{ articles}) \times 4 \text{ hours/article} = 20 \text{ hours}$
- On Tuesday: $(7 \text{ articles}) \times 4 \text{ hours/article} = 28 \text{ hours}$
- On Wednesday: $(14 \text{ articles}) \times 4 \text{ hours/article} = 56 \text{ hours}$

The total number of hours spent writing over the three days is:

$$20 \text{ hours} + 28 \text{ hours} + 56 \text{ hours} = 104 \text{ hours}$$

Thus, the total number of hours spent writing articles in the three days is $\boxed{104}$.